FDG-SPECT: Correlation with FDG-PET

William H. Martin, Dominique Delbeke, James A. Patton, Brian Hendrix, Zeev Weinfeld, Israel Ohana, Robert M. Kessler and Martin P. Sandler

Section of Nuclear Medicine, Department of Radiology and Radiological Sciences, Vanderbilt University Medical Center, Nashville, Tennessee; and Elscint, Inc., Haifa, Israel

The clinical utility of FDG-PET imaging in the evaluation of patients with cardiac, oncologic and neurologic diseases is well documented. The major disadvantages of PET continue to be its high cost and limited availability. **Methods:** With the goal of providing equivalent diagnostic information using a widely available, less expensive modality, we evaluated the clinical utility of FDG-SPECT imaging with a conventional dual-headed camera as compared to PET in 21 patients. **Results:** To compare the image quality of the two modalities, major physical parameters and phantom determinations were obtained. By using the 511-keV collimators, we achieved resolution and system volume sensitivity that were less than those for PET by factors of 2.6 and 8, respectively. The SPECT system, on the other hand, could easily resolve 2 × 0.5-cm cold defects in the heart phantom and 2-cm hot lesions in a 22-cm cylindrical phantom with a target-to-background ratio of 5:1. FDG-SPECT imaging of nine patients with heart disease yielded similar diagnostic information of the amount of viable myocardium present when compared to PET. In seven of eight patients, malignant tissue visualized with FDG-PET was seen equally well with SPECT. The lesions not visualized with FDG-SPECT were either small (≤1.5 cm) or benign. SPECT imaging of four patients with cerebral lesions was inconclusive due to the small sample size but seemed promising. **Conclusion:** FDG-SPECT with 511-keV collimation is less expensive, more available and technically simpler than PET. We believe that FDG-SPECT has achieved sufficient sensitivity and resolution to detect myocardial viability and diagnose malignant tumors ≥2 cm in diameter.

Key Words: fluorine-18-fluorodeoxyglucose; positron emission tomography; single-photon emission computed tomography; coronary artery disease; neoplasm

J Nucl Med 1995; 36:988–995

The clinical utility of PET is well documented, and high-resolution imaging of ^{18}F-fluorodeoxyglucose (^{18}FDG) has been used for many years to study glucose utilization in the brain, heart and neoplasms. In tissues containing low levels of intracellular glucose-6-phosphatase (i.e., brain, heart and striatal muscle), fluorodeoxyglucose is accumulated within cells proportional to the cellular glycotic rate (*1*). In neoplasms, uptake of ^{18}FDG may be a matter of proliferative rate (*2*). The initial application of ^{18}FDG-PET was in the evaluation of seizure disorders, brain tumors and dementia, where it is more sensitive and specific than other imaging modalities (*3–5*). The technique was then applied to the heart, where myocardial viability is virtually assured by significant ^{18}FDG activity measured within a myocardial region demonstrating diminished coronary blood flow, whether by $^{13}NH_3$, ^{201}Tl-chloride, or ^{99m}Tc-sestamibi (MIBI) (*6–8*). Recently, ^{18}FDG-PET studies have proven to be of significant clinical feasibility in oncology, where the malignant potential of a lesion can usually be defined by the degree of ^{18}FDG accumulation within that mass (*9,10*).

Widespread implementation of PET as a clinical imaging modality has been hindered by the high costs of imaging systems ($1–2 million), cyclotrons ($2–3 million), support laboratories ($1–2 million), maintenance and operations ($0.5–1 million) (*11*), and by limited third-party reimbursement. This has stimulated interest in alternative methods of imaging the 511-keV photons of positron emitters (*12,13*). The purpose of this study was to evaluate the clinical feasibility of SPECT imaging of ^{18}FDG with a conventional dual-head gamma camera. If successful, this application would require regional distribution of ^{18}FDG, which has already been accomplished in some areas for PET imaging without in-house cyclotron facilities. Major physical parameters were measured with both the gamma camera and the PET system, and several phantoms were studied to compare the image quality of the two modalities. All the studies were performed with PET and SPECT to compare the clinical diagnostic quality of ^{18}FDG-SPECT.

MATERIALS AND METHODS

Equipment and Physical Measurements

SPECT imaging was performed using an APEX Helix dual-head, rectangular field of view digital scintillation camera (Elscint, Inc., Hackensack, NJ). The camera electronics were modified by the manufacturer to permit imaging of 511-keV photons in the singles mode. The long-range linear response of the Helix front end signal pulse-height electronics enables the acquisition of both linearity and energy correction tables in the standard energy range (30–360 keV) and their application in the ultra-high energy region (511 keV) without degradation in either uniformity or spatial resolution. The electronics are also modified to take maximum advantage of the relatively high signal produced by the 511-keV photons and of the simultaneous 180° photon radiation. These

Received Jul. 12, 1994; revision accepted Oct. 18, 1994.

For correspondence or reprints contact: Martin P. Sandler, MD, Department of Radiology and Radiological Sciences, Vanderbilt University Medical Center, 21st Ave. South & Garland, Nashville, TN 37232-2675.

modifications resulted in a measured energy resolution of 8.5% (FWHM of photopeak) at 511 keV. At this energy, the 3/8 inch thick NaI(Tl) crystals have a photopeak detection efficiency of approximately 13%. A set of ultra-high energy (UHE) collimators were designed to support ultra-high energy, general-purpose, whole body and SPECT applications. The collimators have a core length of 80 mm with 4-mm diameter hexagonal holes and 2.5-mm thick septa. The septal penetration for a single septum between adjacent holes was calculated to be 3.9%. Each collimator weighed 142 kg. The system sensitivity (including collimator penetration) with the UHE collimators was measured with a 10-cm diameter disk source of ^{18}F and with an energy window of 511 keV ± 10% using the NEMA sensitivity protocol. By evaluating detected counts outside of a 10-cm diameter circular region of interest (ROI) over the disk source and contributions to line spread measurements from penetration, an estimate was made of the percentage of detected photons due to penetration. Planar measurements of spatial resolution were made with a thin line source of ^{18}F in air at 0, 5, 10, 15 and 20 cm from the collimator pressure-sensitive device (7 mm from the collimator face). SPECT spatial resolution measurements with scatter were made with a thin line source of ^{18}F in the center of a 22-cm diameter water-filled cylindrical phantom using a 13-cm radius of rotation and a circular orbit. A Hamming filter was used for image reconstruction to optimize spatial resolution measurements. SPECT volume sensitivity measurements using both heads were made with a 22-cm diameter cylindrical phantom containing a solution of ^{18}F and using a 13-cm radius of rotation and a circular orbit. The digital electronics of the camera permitted frame-by-frame decay correction for short-lived radioisotopes like ^{18}F.

PET imaging was performed using an ECAT 933/08/16 tomograph (CTI/Siemens, Knoxville, TN) with a 12.8-cm axial field of view, producing 15 transaxial slices, each of 8-mm thickness. Spatial resolution and volume sensitivity measurements were made using the same protocol as with the dual-head camera. For the volume sensitivity determination, measured counts were related to the actual activity within the field of view since the phantom was longer than the axial field of view. A Hamming filter was used for all image reconstructions except the spatial resolution measurement where a ramp filter was used to optimize resolution. The scanner hardware estimates and corrects for random events using the standard delayed window technique.

Image acquisitions of 30 min duration were performed on both systems using a Data Spectrum cardiac phantom (Chapel Hill, NC) containing 300 μCi of ^{18}F and placed in a 22-cm diameter water-filled cylindrical phantom. The phantom contained two simulated 45° defects: one 2 × 1 cm, and the other 2 × 0.5 cm.

To evaluate the ability of the camera system to detect hot lesions, a 22-cm diameter phantom containing six spheres of diameter ranging from 1.3 to 3.8 cm was imaged with the PET scanner and the dual-head camera. Both the phantom and the spheres were filled with a solution containing ^{18}F, with the concentrations adjusted to provide a ratio of sphere activity-to-background activity of 5:1 in order to simulate clinical situations involving hot lesion detection. The phantom was imaged on the PET scanner for 10 min and the dual-head SPECT camera for 60 min to make approximate adjustments for differences in system sensitivity. Circular ROIs, the size of the smallest sphere, were identified over each sphere and a background area over the volume, and contrast ratios of measured sphere counts to background counts were calculated and tabulated.

Patients

The study group was made up of 21 patients who underwent clinical ^{18}FDG-PET imaging followed immediately by ^{18}FDG-SPECT of the same region. Group 1 included nine patients being evaluated for myocardial viability; Group 2 consisted of eight patients being assessed for malignant tumors and Group 3 included four patients being assessed for intracerebral lesions.

All Group 1 patients had undergone routine evaluation of myocardial perfusion with ^{201}Tl SPECT, ^{99m}Tc-MIBI SPECT or $^{13}NH_3$ PET, as well as percutaneous coronary angiography. Patients in Group 2 had been assessed previously with various modalities, including CT and/or MRI. Patients with hepatic metastases had undergone CT arterial portography. The Group 3 patients were all assessed with MRI and/or CT of the brain.

FDG-PET Imaging

All patients were fasted for a minimum of 4 hr prior to imaging. Transmission scans (10 min per bed position) were obtained in all patients using a ring source of ^{68}Ge to correct for photon attenuation followed by intravenous administration of approximately 370 MBq (10 mCi) ^{18}FDG. After a 45–60-min distribution phase, emission imaging was performed for 15 min per bed position. A stationary laser system was used to ensure accurate positioning between transmission and emission scanning.

Group 1 patients were loaded with 50 g oral glucose 45–60 min prior to injection of ^{18}FDG. Two patients underwent a PET perfusion study using $^{13}NH_3$ on the same day as their ^{18}FDG study. Group 2 patients were scanned with two to five nonoverlapping sets of transaxial images. Group 3 patients were scanned with two interleaved bed positions, yielding slices of 8-mm thickness with 4 mm of overlap. A thermoplastic face mask, molded to the patient's head and locked into the head holder of the scanner, was used to minimize head movement during brain imaging. Images were obtained in the axial plane and then reconstructed in both the coronal and sagittal planes.

SPECT Imaging

All patients were imaged using the dual-head scintillation camera immediately following completion of PET imaging, ranging from 60 to 150 min after ^{18}FDG injection depending on the number of bed positions imaged with PET.

The SPECT acquisition protocol for the Group 1 patients included a single-head rotating 180° from the RAO (315°) to the LPO (135°) projection for 60 stops at 30 sec per stop. Initial cardiac studies were performed by collecting data from both heads, and two sets of images were reconstructed: one set using data from both heads and the second set using data from only the head rotating from the RAO to LPO position. Comparison of the two image sets showed that the dataset from the single-head was slightly superior in resolution to that from the dual-head set, and therefore the remainder of the study was conducted with the single-head. Geometric attenuation corrections were applied to the first studies but yielded no improvement in image quality. The images were collected in a 64 × 64 matrix using word mode and then reconstructed using a Butterworth filter and temporal smoothing along the short axis, the horizontal long axis, and the vertical long axis of the heart. For the remaining patients, each head acquired images every 3° for 180° over the ROI in a 64 × 64 matrix. Frame-by-frame decay correction was performed before image reconstruction was accomplished. Geometric attenuation corrections were performed on the brain images.

This protocol was approved by the VUMC Institutional Review Board, and all participants gave written informed consent.

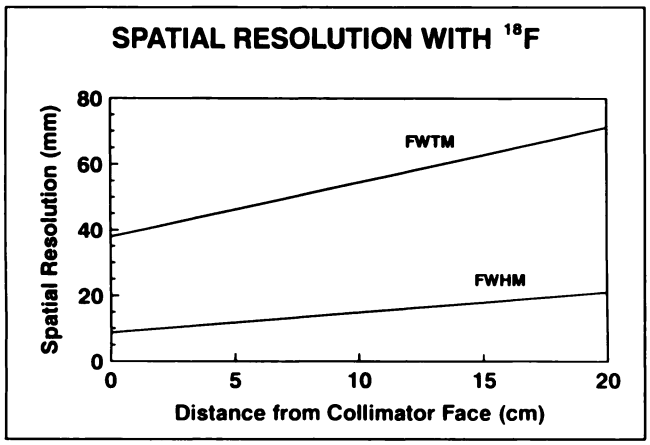

FIGURE 1. Spatial resolution (FWHM and FWTM) measurements made with a line source of ^{18}F in air for the ultra-high energy (UHE) collimator.

TABLE 1
Measured Contrast Ratios of Hot Spheres in a Warm Background

Sphere diameter (cm)	Measured contrast ratio ± s.e.	
	PET	Dual-head camera
3.8	4.84 ± 0.09	3.13 ± 0.24
3.2	4.93 ± 0.09	2.64 ± 0.21
2.5	4.54 ± 0.08	2.13 ± 0.17
1.9	3.44 ± 0.06	1.65 ± 0.14
1.6	2.74 ± 0.05	1.18 ± 0.11
1.3	2.06 ± 0.04	1.11 ± 0.10

Sphere and background concentrations were 13.66 and 2.73 μCi/ml for the PET measurements and 10.61 and 2.12 μCi/ml for the dual-head camera measurements.

Image Analysis

For the cardiac patients (Group 1), images of all PET and SPECT scans were reoriented along the short axis of the heart with slices of the same thickness. Three sets of short-axis images from ^{201}Tl-SPECT (or $^{13}NH_3$ PET/^{99m}Tc-MIBI), ^{18}FDG-PET and ^{18}FDG-SPECT were compared separately and independently by two experienced observers. Side-by-side comparisons of the relevant images were then made by each observer, and differences were resolved by consensus.

In each patient, the myocardial region with the maximum counts on the ^{201}Tl/^{99m}Tc-MIBI/$^{13}NH_3$ study was used as the normal perfusion reference for that patient. The myocardial segment on the ^{18}FDG images that corresponded to the normal perfusion reference on the ^{201}Tl/^{99m}Tc-MIBI/$^{13}NH_3$ images was used as the normal reference region for relative ^{18}FDG uptake. In all other myocardial regions, ^{18}FDG uptake was compared to the activity in this normal reference region. The activity of ^{18}FDG was determined to be either normal (normal perfusion associated with normal ^{18}FDG activity), matched (diminished relative ^{18}FDG activity with reduced perfusion) or mismatched (increased relative ^{18}FDG activity with reduced perfusion).

Side-by-side comparisons of the ^{18}FDG-PET and ^{18}FDG-SPECT images of the oncology (Group 2) and neurology (Group 3) patients were made. Differences were graded per detected lesion on a three-point scale (3 = no or minimal difference, 2 = mild difference but clinically insignificant, 1 = moderate to marked clinically significant difference). The standard uptake value (SUV) was calculated for all lesions >1.2 cm as follows: lesion activity (μCi/ml) ÷ dose (mCi)/body wt (kg). Lesion size was determined from contemporary CT scans.

RESULTS

Physical Measurements

The system sensitivity for the dual-head camera with the UHE collimators was measured to be 129 cpm/μCi with a 10-cm diameter disk source of ^{18}F. By evaluating detected counts outside of a 10-cm diameter circular ROI over the disk source and contributions to line spread measurements from penetration, it was estimated that approximately 52% of the detected photons were due to penetration. Therefore, excluding penetration, the system sensitivity was calculated to be 62 cpm/μCi. Planar spatial resolution measurements with a thin line source of ^{18}F yielded the FWHM and FWTM values shown in Figure 1. SPECT spatial resolution measurements with scatter yielded a measurement of 17 mm FWHM. SPECT volume sensitivity measurements yielded a value of 270 cpm/μCi.

For the PET scanner, the spatial resolution within an 8-mm slice was measured to be 6.5 mm, yielding a voxel size of 6.5 × 6.5 × 8 mm. The volume sensitivity was

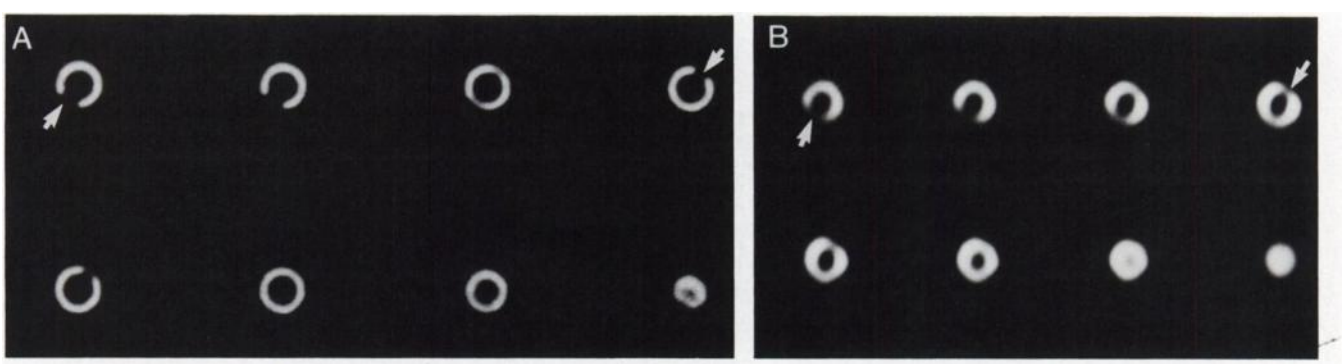

FIGURE 2. Short-axis slices of 8-mm thickness obtained with the Data Spectrum cardiac phantom with two 45° lesions (2 × 1 cm and 2 × 0.5 cm) (arrows) and placed in a 22-cm diameter water-filled phantom. Thirty-minute scans were performed with the PET scanner (A) and the dual-head camera (B) with the cardiac phantom containing 300 μCi of ^{18}F.

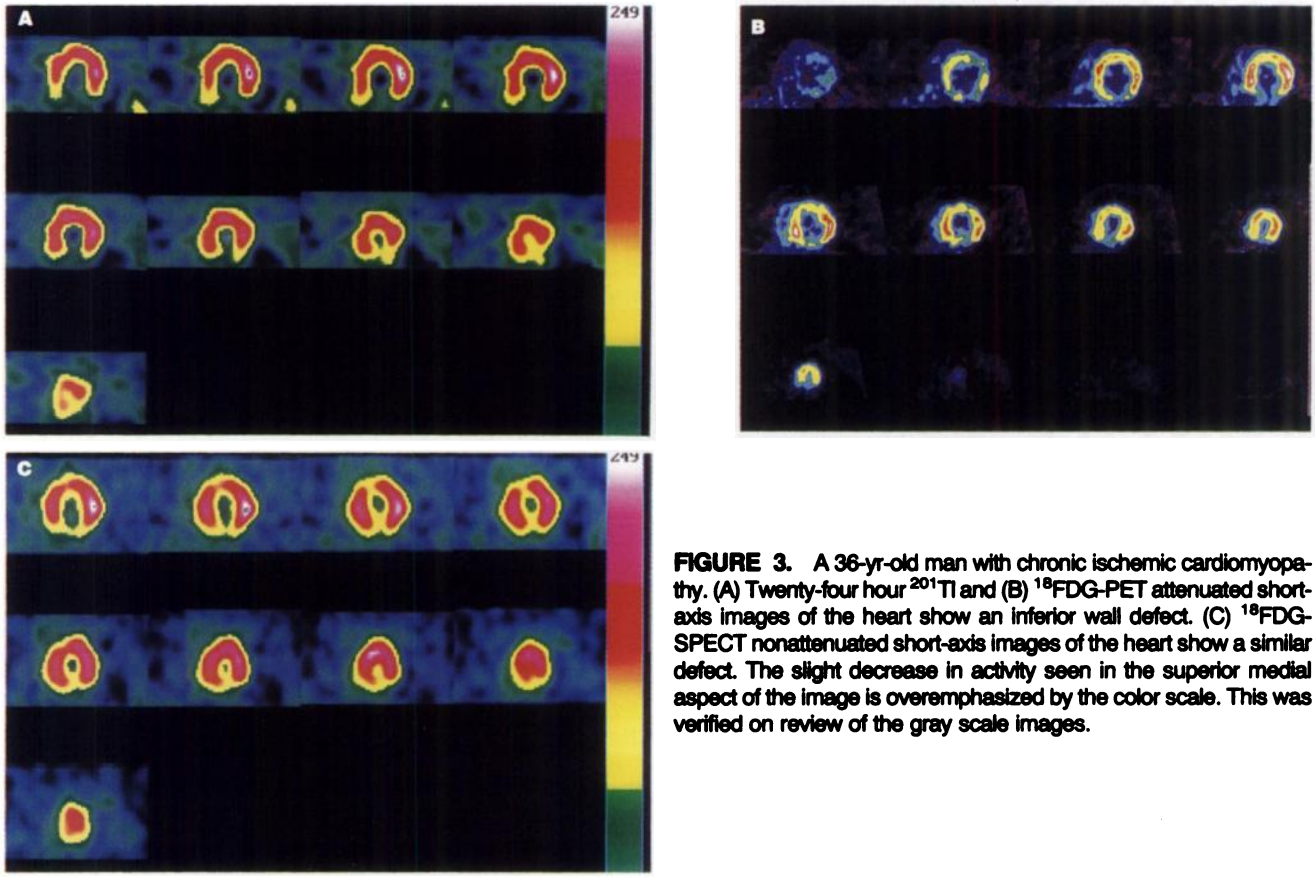

FIGURE 3. A 36-yr-old man with chronic ischemic cardiomyopathy. (A) Twenty-four hour ^{201}Tl and (B) ^{18}FDG-PET attenuated short-axis images of the heart show an inferior wall defect. (C) ^{18}FDG-SPECT nonattenuated short-axis images of the heart show a similar defect. The slight decrease in activity seen in the superior medial aspect of the image is overemphasized by the color scale. This was verified on review of the gray scale images.

measured to be 2238 cpm/μCi. When comparing dual-head SPECT to PET for 511-keV imaging, it is apparent that the measured spatial reconstructed resolution is less by a factor of 2.6, and volume sensitivity is less by a factor of 8.

Figure 2 shows comparable images of 8-mm thick slices in the short-axis view of the Data Spectrum cardiac phantom. The superior spatial resolution of PET is apparent in the thin, well-defined walls of the phantom (1 cm thick) and in the definition of the two lesions. The images from the dual-head camera, however, clearly define both lesions and show that the dual-head camera with the 511-keV collimator can resolve cold defects of 2 × 0.5 cm in the heart.

Contrast ratios (and errors based on ROI counts) calculated for the hot lesions in a warm background are shown in Table 1 along with the actual concentrations at the time of the measurements. The data show that the measured contrast ratios obtained with PET are superior to those obtained with the dual-head camera. This is to be expected due to the superior resolution of PET. The theory of hot spot recovery coefficients and contrast recovery coefficients (*14*) predicts that absolute recovery of contrast can only be obtained for spherical lesions that have diameters of at least three times the FWHM of the imaging system. This theory would predict absolute recovery by PET (FWHM of 8 mm) for lesions of 2.4 cm diameter and larger, and by SPECT (FWHM of 17 mm) for lesions of 5.1 cm diameter and larger. Hot lesion detectibility, however, is determined by lesion uptake, and the phantom data predict that lesions ≥2 cm with uptake ratios of 5:1 can be detected with the dual-head camera, assuming adequate counting statistics in the images.

Clinical Results

Group 1. Eight of nine cardiac patients had matching perfusion and metabolic defects consistent with prior infarctions (Fig. 3), and four patients also had separate areas of mismatch consistent with hibernating myocardium. A heart transplant patient had no significant metabolic abnormality. The number, size and distribution of metabolic defects seen with ^{18}FDG imaging were similar with SPECT and PET. The ^{18}FDG-SPECT images were all of excellent quality, although the resolution of the PET images was slightly superior to those of ^{18}FDG-SPECT. In all nine patients, the clinical assessment as to the amount of viable myocardium present was similar with SPECT and PET.

Group 2. In seven of eight patients, neoplastic tissue visualized with ^{18}FDG-PET was visualized with subsequent ^{18}FDG-SPECT as well or almost as well (scores 3–2) (Figs. 4–5). One patient evaluated for elevated catecholamines demonstrated a small area of mildly increased activity in the mid-left lung field with ^{18}FDG-PET (SUV = 2.4), which corresponded to a benign fibronodular infiltrate on CT extending over 2 × 4 cm. This benign lesion was not visualized with ^{18}FDG-SPECT. Twelve malignant lesions were detected by ^{18}FDG-PET in seven patients. Ten malignant lesions were detected by ^{18}FDG-SPECT in six pa-

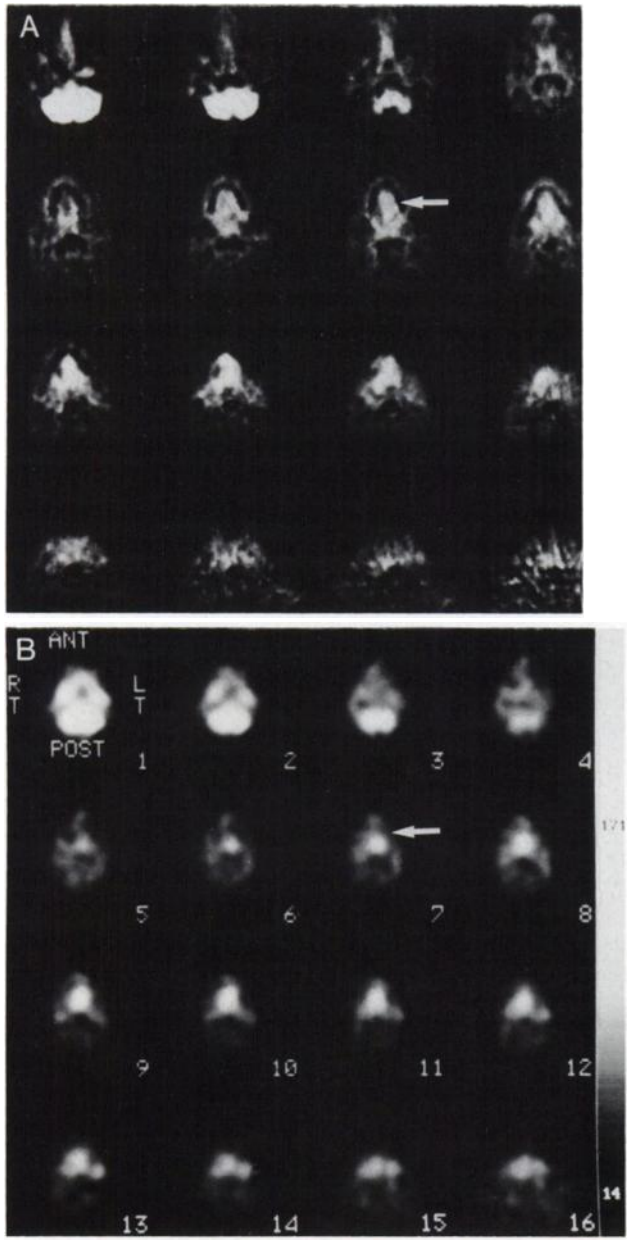

FIGURE 4. A 41-yr-old man with a recurrent squamous-cell carcinoma of the tongue, irradiated 3 mo prior to the scan. (A) ^{18}FDG-PET: axial images show an area of increased uptake in the region of the posterior tongue (arrow). (B) ^{18}FDG-SPECT: axial images show the same area of increased uptake as the ^{18}FDG-PET scan (arrow).

tients. In one patient with adenocarcinoma who had multiple hepatic metastases of <1.5 cm demonstrated by MRI, two lesions were faintly visualized by ^{18}FDG-PET. An accurate standard uptake ratio for these two lesions could not be calculated because of their small size and central necrosis. These were the only malignant lesions not visualized with ^{18}FDG-SPECT.

Group 3. Of the four patients who underwent brain imaging, none demonstrated a hypermetabolic focus on ^{18}FDG-PET or ^{18}FDG-SPECT. A typical brain scan is shown in Figure 6. In one patient, a 1-cm brainstem lesion, most consistent with either infarction or a low-grade glioma, could not be identified on ^{18}FDG-PET or ^{18}FDG-SPECT. A 2-cm rim-enhancing cerebellar lesion was identified as hypometabolic with ^{18}FDG-PET, but could not be visualized with ^{18}FDG-SPECT against the warm background of the cerebellum in an AIDS patient. In two patients, postsurgical hypometabolic regions were identified with both ^{18}FDG-PET and ^{18}FDG-SPECT, with no areas of high-grade tumor recurrence visualized in either patient. Physiologic ^{18}FDG uptake allowed good delineation of basal ganglia, thalamus and cortical detail in all patients with both PET and SPECT, although the resolution of the PET images was distinctly superior.

Summary of Results

The diagnostic information obtained from the studies of the cardiac patients demonstrated no significant advantage of PET versus ^{18}FDG-SPECT. Seven of the eight oncology patients studied demonstrated concordance between the PET and SPECT images. The lesions not visualized in the Group 2 patients with ^{18}FDG-SPECT were ≤1.5 cm in diameter with central necrosis and one larger benign lesion with a relatively low ^{18}FDG uptake. Our ^{18}FDG-SPECT data from the Group 3 patients are inconclusive and require a larger series of patients.

DISCUSSION

The purpose of this study was to assess the feasibility of using specially designed 511-keV collimators for ^{18}FDG-SPECT imaging with the APEX Helix dual-head gamma camera (Elscint). All patients underwent PET imaging prior to imaging with the APEX Helix due to constraints imposed by the approved Institutional Review Board protocol. Therefore, the activity of ^{18}F at the time of SPECT imaging was always less (sometimes <50%) than that at the time of PET imaging. The study group consisted of 21 patients with a variety of cardiac, oncologic and neurologic diseases.

Imaging of the heart with PET and ^{18}FDG-SPECT provided equivalent diagnostic information regarding myocardial viability. As reviewed by Go et al. (*15*), the higher accuracy of PET as compared to ^{201}Tl-SPECT is related to both enhanced contrast (not spatial) resolution and accurate attenuation correction. In contrast to ^{201}Tl-SPECT, the high energy of ^{18}F results in excellent image contrast with ^{18}FDG-SPECT similar to PET. The larger field of view of the APEX Helix (40 cm) when imaging patients with cardiomegaly simplifies positioning in comparison to PET. Other investigators have reported success with both planar and ^{18}FDG-SPECT imaging of the heart (*12,16–18*). Preliminary outcome data reported by Bax et al. (*17*) indicate that ^{18}FDG-SPECT may be comparable to ^{18}FDG-PET (*6*) in predicting myocardial recovery following revascularization. Despite the use of more complex imaging protocols, both ^{201}Tl and ^{99m}Tc-MIBI SPECT continue to underestimate myocardial viability (*7,8,19–22*). The data in this report and that of others (*12,16–18*) indicate that

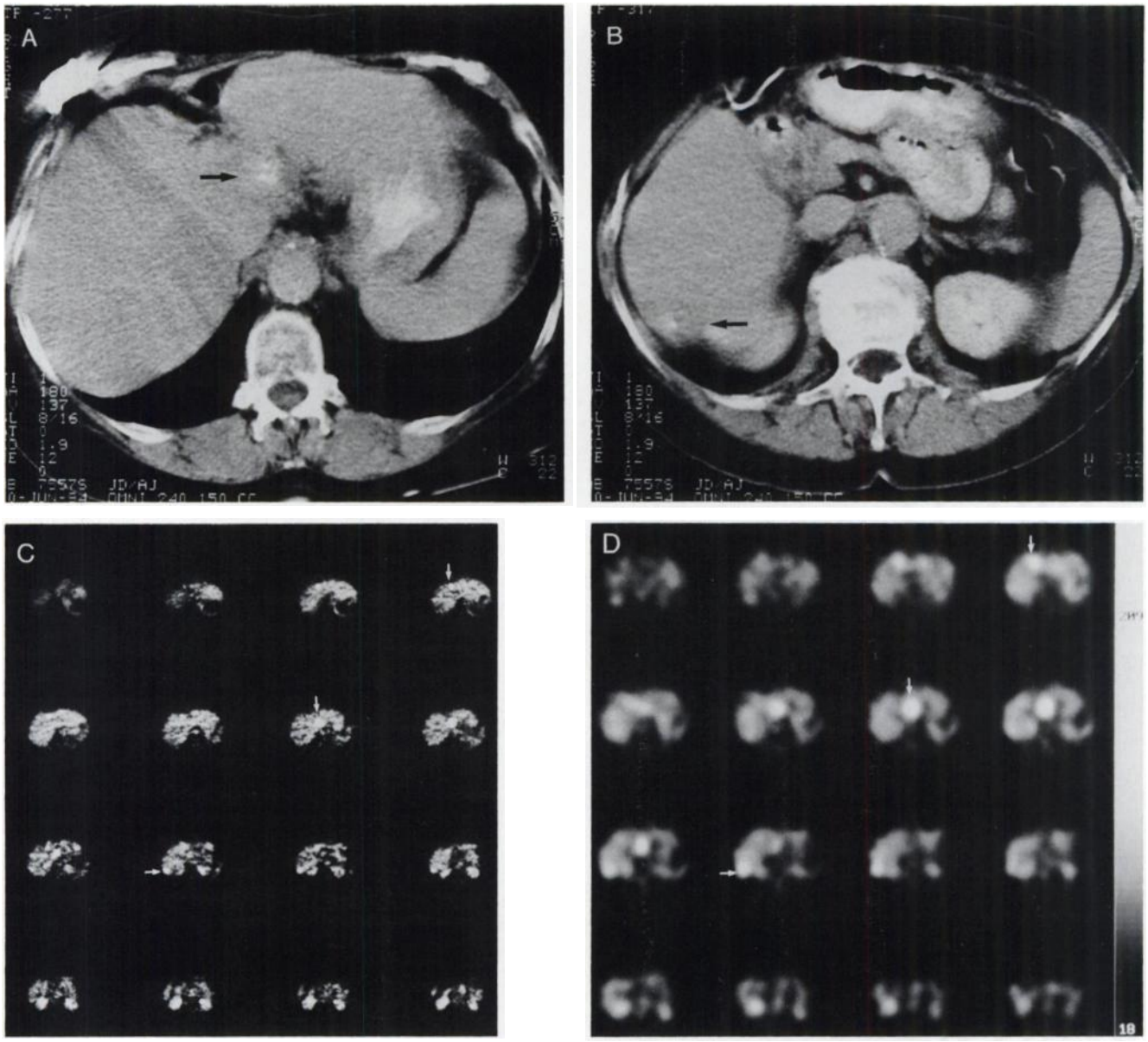

FIGURE 5. A 66-yr-old woman with colon carcinoma metastatic to the liver and prior partial hepatectomy. (A,B) CT scans show two lesions (arrows) with calcification in the liver (2 cm, 2.7 cm). (C) ^{18}FDG-PET: transaxial images of the liver show increased uptake corresponding to the two lesions scanned on CT plus an additional lesion in the region of her prior resection (arrows). SUV 4.5–6.7. (D) ^{18}FDG-SPECT: transaxial images of the liver show three hypermetabolic lesions.

^{18}FDG-SPECT is of equal utility to PET for assessment of myocardial viability.

Numerous other investigators have reported detection of malignancies using ^{18}FDG-SPECT imaging with variable success (*12,23,24*). The generally high tumor-to-background ratio of ≥3:1 (frequently 10:1) seen with ^{18}FDG imaging of malignant tumors (*25,26*) represents a significant advantage of oncology imaging with ^{18}FDG. As demonstrated with our hot sphere phantom data, tumors with a ratio of 5:1 should be visible if ≥2.0 cm in diameter, assuming adequate counting statistics in the image. The detectibility of malignant neoplasms with ^{18}FDG, however, depends not only on size but also on intensity of ^{18}FDG uptake, degree of central necrosis, tumor depth and contrast with surrounding structures. The only tumors not detected by ^{18}FDG-SPECT in this study were small (≤1.5 cm) and demonstrated decreased ^{18}FDG uptake due to central necrosis or benignity. Malignant tumors larger than 2 cm were detected equally by both PET and SPECT. As demonstrated in Figure 5, ^{18}FDG-SPECT in certain circumstances may be more accurate than CT in determining tissue malignancy (*27,28*). Quantitation of activity utilizing the SUV is inaccurate when examining tumors <2 cm due to volume averaging errors (*28*).

The limited resolution of ^{18}FDG-SPECT provides a significant challenge for imaging small intracerebral lesions. Based on phantom data and the limited data in this study, ^{18}FDG-SPECT should be helpful in differentiating high-

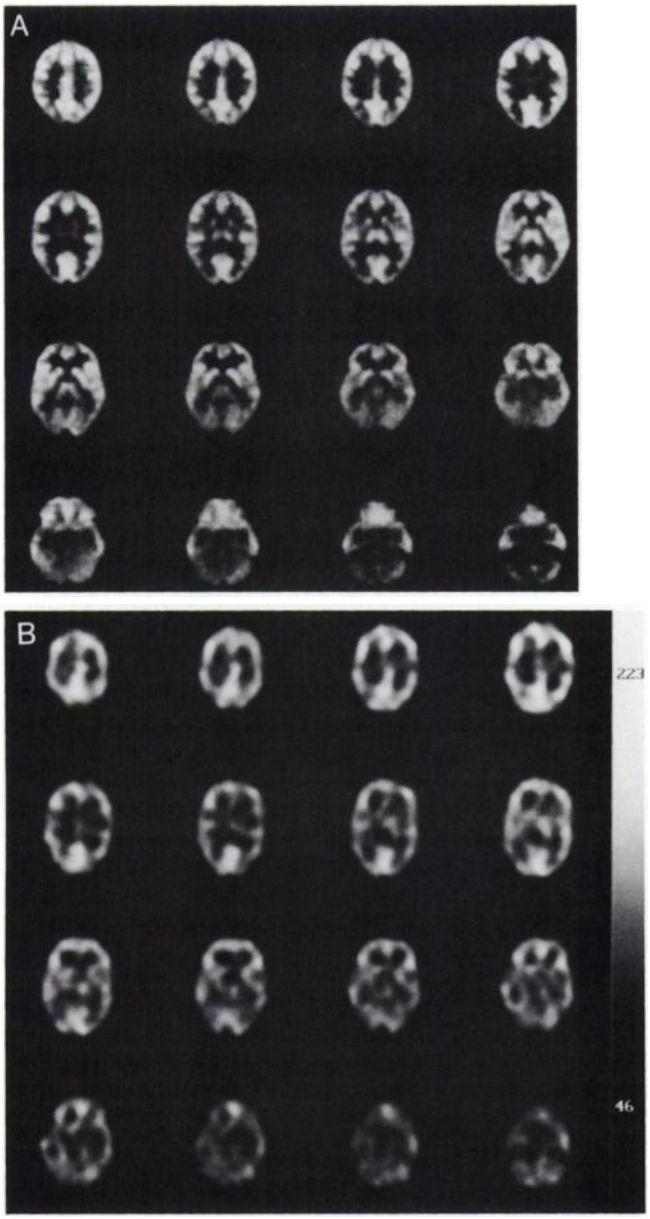

FIGURE 6. Typical ^{18}FDG brain scan without lesions in the field of view. (A) ^{18}FDG-PET and (B) ^{18}FDG-SPECT.

grade from low-grade lesions of >2 cm in diameter. Since ^{99m}Tc-HMPAO-SPECT has been effective in the evaluation of dementia and seizure patients (*4,29,30*), we would expect ^{18}FDG-SPECT to be similarly efficacious; but until these studies are completed, PET imaging of the brain continues to have a significant advantage over ^{18}FDG-SPECT.

With PET, the ideal time for imaging is reported to be 50–70 min after ^{18}FDG administration. The delay in SPECT imaging mandated by the design of our study did not result in any apparent degradation of image quality. While extending the time for imaging beyond 90 min will diminish the count density, the tumor-to-background ratio may actually increase (*25,28*). The optimal acquisition time for ^{18}FDG-SPECT imaging awaits further study. Although a thicker crystal might be advantageous for 511-keV imaging due to increased efficiency, it would hinder the use of the camera for other routine imaging applications with standard low-energy radioisotopes.

CONCLUSION

Our data and that of others suggest that ^{18}FDG-SPECT imaging has achieved sufficient sensitivity and resolution to enable detection of hibernating myocardium (*12,16–18*). The detection of malignant neoplasms with ^{18}FDG-SPECT is possible for non-necrotic tumors of ≥2 cm in diameter assuming adequate uptake in the tumor.

PET continues to be more advantageous than ^{18}FDG-SPECT in its ability to detect small tumors and remains a powerful research modality with greater access to physiological and biochemical pathways and their measurements, including receptor systems, than any other currently available in vivo imaging modality.

ACKNOWLEDGMENTS

The authors wish to express their appreciation to Virginia Brocker and Tom Ebers for preparation of the manuscript. They also thank John Bobbitt for his production of the figures.

The authors would also like to recognize the assistance of Tommy Schwarz, Director of Sales and Marketing for Elscint, Inc. His insight, support and positive attitude were invaluable to this project. His recent death in a tragic accident is a loss for all of us. He will be missed.

REFERENCES

1. Som P, Atkins HL, Bandoypadhyay D, et al. A fluorinated glucose analog, 2-fluoro-2-deoxy-D-glucose (F-18): nontoxic tracer for rapid tumor detection. *J Nucl Med* 1980;21:670–675.
2. Kubota R, Kubota K, Yamada S, Tada M, Ido T, Tamahashi N. Active and passive mechanisms of [fluorine-18]fluorodeoxyglucose uptake by proliferating and necrobiotic cancer cells in vivo: a microautoradiographic study. *J Nucl Med* 1994;35:1067–1075.
3. DeChiro G. Positron emission tomography using ^{18}F-fluorodeoxyglucose in brain tumors. *Invest Radiol* 1987;22:360–371.
4. Coubes P, Awad IA, Antar M, Magdinec M, Sufka B. Comparison and spatial correlation of interictal HMPAO-SPECT and FDG-PET in intractable temporal lobe epilepsy. *Neurol Res* 1993;15:160–168.
5. Weinstein HC, Scheltens P, Hijdra W, van Royen EA. Neuro-imaging in the diagnosis of Alzheimer's disease. II. Positron and single photon emission tomography. *Clin Neurol Neurosurg* 1993;95:81–91.
6. Tillisch J, Brunken R, Marshall R, et al. Reversibility of cardiac wall motion abnormalities predicted by positron tomography. *N Engl J Med* 1986;314:884–888.
7. Bonow RO, Dilsizian V, Cuocolo A, Bacharach SL. Identification of viable myocardium in patients with chronic coronary artery disease and left ventricular dysfunction: comparison of thallium scintigraphy with reinjection and PET imaging with ^{18}F-fluorodeoxyglucose. *Circulation* 1991;83:26–37.
8. Altehoefer C, Kaiser HJ, Dörr R, et al. Fluorine-18-deoxyglucose PET for assessment of viable myocardium in perfusion defects in ^{99m}Tc-MIBI SPECT: a comparative study in patients with coronary artery disease. *Eur J Nucl Med* 1992;19:334–342.
9. Okada J, Yoshikawa K, Itami M, et al. Positron emission tomography using fluorine-18-fluorodeoxyglucose in malignant lymphoma: a comparison with proliferative activity. *J Nucl Med* 1992;33:325–329.
10. Strauss LG, Clorius JH, Schlag P, et al. Recurrence of colorectal tumors: PET evaluation. *Radiology* 1989;170:329–332.
11. Conti PS, Keppler JS, Halls JM. Positron emission tomography: a financial and operational analysis. *AJR* 1994;162:1279–1286.
12. Drane WE, Abbott FD, Nicole MW, Mastin ST, Kuperus JH. Technology for FDG SPECT with a relatively inexpensive gamma camera. *Radiology* 1994;191:461–465.

13. van Lingen A, Huijgens PC, Visser FC, et al. Performance characteristics of a 511-keV collimator for imaging positron emitters with a standard gamma camera. *Eur J Nucl Med* 1992;19:315–321.
14. Kessler RM, Ellis JR, Eden M. Analysis of emission tomographic scan data: limitations imposed by resolution and background. *J Comput Assist Tomogr* 1984;8:514–522.
15. Go RT, MacIntyre WJ, Chen EQ, Cook SA, Neumann DR, Saha GB. Current status of the clinical applications of cardiac positron emission tomography. *Radiol Clin N Am* 1994;32:501–519.
16. Oppenheim BE, Burt RW, Schauwecker DS. Comparison of a three detector gamma camera and a PET scanner for performing F-18-FDG cardiac scintigraphy [Abstract]. *J Nucl Med* 1994;35(suppl):111P.
17. Bax JJ, Cornel JH, Visser FC, et al. Reversibility of wall motion abnormalities predicted by SPECT with F-18-fluorodeoxyglucose [Abstract]. *J Nucl Med* 1994;35(suppl):136P.
18. Burt RW, Perkins OW, Oppenheim BE, et al. Comparison of rest thallium SPECT, F-18 FDG PET and F-18 FDG SPECT for evaluation of myocardial viability [Abstract]. *J Nucl Med* 1994;35(suppl):49P.
19. Tamaki N, Ohtani H, Yamashita K, et al. Metabolic activity in the areas of new fill-in after thallium-201 reinjection: comparison with positron emission tomography using fluorine-18-deoxyglucose. *J Nucl Med* 1991;32:673–678.
20. Dilsizian V, Rocco TP, Freedman NMT, et al. Enhanced detection of ischemic but viable myocardium by the reinjection of thallium after stress-redistribution imaging. *N Engl J Med* 1990;323:141–146.
21. Rocco TP, Dilsizian V, Strauss HW, et al. Technetium-99m isonitrile myocardial uptake at rest. II. Relation to clinical markers of potential viability. *J Am Coll Cardiol* 1989;14:1678–1684.
22. Cuocolo A, Pace L, Ricciardelli B, et al. Identification of viable myocardium in patients with chronic coronary artery disease: comparison of thallium-201 scintigraphy with reinjection and technetium-99m-methoxyisobutyl isonitrile. *J Nucl Med* 1992;33:505–511.
23. Hoekstra OS, van Lingen A, Ossenkoppele GJ, Golding R, Teule GJ. Early response monitoring in malignant lymphoma using fluorine-18 fluorodeoxyglucose single-photon emission tomography. *Eur J Nucl Med* 1993;20:1214–1217.
24. MacFarland D, Cotton L, Ackerman R, Minn H, Ficaro E, Wahl RL. Triple-head FDG-SPECT: initial evaluation in oncology and comparison to FDG-PET [Abstract]. *J Nucl Med* 1994;35(suppl):7P.
25. Wahl RL, Harney J, Hutchins G, Grossman HB. Imaging of renal cancer using positron emission tomography with 2-deoxy-2-(^{18}F)-fluoro-D-glucose: pilot animal and human studies. *J Urol* 1991;146:1470–1474.
26. Newman JS, Francis IR, Kaminski MS, Wahl RL. Imaging of lymphoma with PET with 2-[F-18]-fluoro-2-deoxy-D-glucose: correlation with CT. *Radiology* 1994;190:111–116.
27. Wahl RL, Cody RL, Hutchins GD, Mudgett EE. Primary and metastatic breast carcinoma: initial clinical evaluation with PET with the radiolabeled glucose analogue 2-[F-18]-fluoro-2-deoxy-D-glucose. *Radiology* 1991;179:765–770.
28. Gritters LS, Francis IR, Zasadny KR, Wahl RL. Initial assessment of positron emission tomography using 2-fluorine-18-fluoro-2-deoxy-D-glucose in the imaging of malignant melanoma. *J Nucl Med* 1993;34:1420–1427.
29. Messa C, Perani D, Lucignani G, et al. High-resolution technetium-99m-HMPAO SPECT in patients with probable Alzheimer's disease: comparison with fluorine-18-FDG PET. *J Nucl Med* 1994;35:210–216.
30. Andersen AR, Waldemar G, Dam M, Fuglsang-Frederiksen A, Herning M, Kruse-Larsen C. SPECT in the presurgical evaluation of patients with temporal lobe epilepsy—a preliminary report. *Acta Neurochir* 1990;50(suppl):80–83.